




**Phononic heat conductance of gold atomic contacts: Coherent versus incoherent transport**F. Müller <sup>1</sup>, P. Nielaba,<sup>1</sup> J. C. Cuevas <sup>2</sup>, and F. Pauly <sup>3</sup><sup>1</sup>*Department of Physics, University of Konstanz, D-78457 Konstanz, Germany*<sup>2</sup>*Departamento de Física Teórica de la Materia Condensada and Condensed Matter Physics Center (IFIMAC), Universidad Autónoma de Madrid, E-28049 Madrid, Spain*<sup>3</sup>*Institute of Physics and Centre for Advanced Analytics and Predictive Sciences, University of Augsburg, D-86159 Augsburg, Germany*

(Received 19 August 2022; accepted 20 October 2022; published 1 November 2022)

We present here a theoretical method to determine the phononic contribution to the thermal conductance of nanoscale systems in the phase-coherent regime. Our approach makes use of classical molecular dynamics (MD) simulations to calculate the temperature-dependent dynamical matrix, and the phononic heat conductance is subsequently computed within the Landauer-Büttiker formalism with the help of nonequilibrium Green's function techniques. Tailored to nanostructures, crucial steps of force constant and heat transport calculations are performed directly in real space. As compared to conventional density functional theory (DFT) approaches, the advantage of our method is twofold. First, interatomic interactions can be described with the method of choice. Semiempirical potentials may lead to large computational speedups, enabling the study of much larger systems. Second, the method naturally takes into account the temperature dependence of atomic force constants, an aspect that is ignored in typical static DFT-based calculations. We illustrate our method by analyzing the temperature dependence of the phononic thermal conductance of gold (Au) chains with lengths ranging from 1 to 12 atoms. Moreover, in order to evaluate the importance of anharmonic effects in these atomic-scale wires, we compare the phase-coherent approach with nonequilibrium MD (NEMD) simulations. We find that the predictions of the phase-coherent method and the classical NEMD approach largely agree above the Debye temperature for all studied chain lengths, which shows that heat transport is coherent and that our phase-coherent approach is well suited for such nanostructures.

DOI: [10.1103/PhysRevB.106.195401](https://doi.org/10.1103/PhysRevB.106.195401)**I. INTRODUCTION**

Understanding and controlling heat transport due to phonons in nanoscale systems and devices is of major importance in a variety of disciplines [1–3]. Very recent experimental advances in nanothermometry have finally pushed thermal conductance measurements all the way down to the scale of single atoms and molecules [4–7]. Special attention has been paid to the case of metallic atomic-size contacts, which are known to be ideal systems to test basic theories of the transport of charge and energy at the nanoscale [8,9]. In this respect, numerous transport properties have been thoroughly analyzed in the context of these atomic-scale wires such as electrical conductance [10,11], shot noise [12–15], photocurrent [16–19], thermopower [20–23], Joule heating [24,25], or Peltier cooling [26], just to mention a few.

The description of the heat conductance of metallic atomic contacts requires the use of fully atomistic methods [4,27–29]. In particular, these methods have explained the observation of thermal conductance quantization in Au single-atom contacts and the fact that the Wiedemann-Franz law, which relates the electrical and thermal conductances in metallic systems, is approximately fulfilled irrespective of the size and material of the atomic contacts [4,27]. These theoretical approaches show for metallic atomic contacts that electrons largely determine the thermal conductance compared to

phonons, similar to the situation in bulk metals. This insight was not obvious a priori because the transport mechanisms for fermionic electrons and bosonic phonons are fundamentally different in these nanoscale systems, as compared to bulk wires. Indeed, Ref. [27] predicts that for aluminum single-atom contacts, phonon thermal transport may contribute as much as 40% to the total thermal conductance, yielding a substantial deviation from the Wiedemann-Franz law. This interesting theoretical prediction, which presently lacks experimental confirmation, shows that these metallic nanowires are still very interesting from the point of view of phonon transport.

Most theoretical calculations of the phonon contribution to the heat conductance of metallic atomic-size contacts assume that transport is fully coherent [4,27,28], i.e., that the inelastic mean free path for phonons is larger than the contact size. Other calculations [29] use the classical Fourier's law, which includes anharmonic transport mechanisms. For single-atom contacts the coherent assumption appears to be reasonable. However, this is not obvious for longer and thicker junctions, since it is known that phonon mean free paths in metals can be as small as a few nanometers [30]. Although the *ab initio* methods based on DFT, which are used so far [4,27,28], are very accurate, they are computationally demanding. Therefore their use is practically restricted to relatively small contacts. In this respect, it would be useful to develop more efficient

methods to describe the phonon transport in systems consisting of many atoms and to shed new light on the role of inelastic interactions.

In this work, we present an efficient method to compute the phononic heat conductance of any kind of nanojunction in the coherent transport regime. This method is based on the calculation of relevant atomic force constants, making use of classical MD simulations in thermal equilibrium, while the phonon transmission and related heat conductance are computed in the framework of the Landauer-Büttiker picture with the help of nonequilibrium Green's function techniques. The approach detailed here considers the temperature dependence of the atomic force constants, which is in general important to describe the temperature dependence of the phononic heat conductance. We present a study of the phononic contribution to the thermal conductance of Au chains in the phase-coherent regime, systematically changing the length of the central chain of the junction. Moreover, we present a comparison of these calculations, which assume harmonic lattice distortions, with the results obtained using a recently developed procedure based on classical NEMD simulations that includes inelastic effects, originating from anharmonic phonon-phonon scattering [29]. This comparison allows us to test the accuracy of the phase-coherent approach for the description of phonon transport in these metallic nanoscale wires and provides insights into the regime, in which the harmonic description is valid. We will show that the coherent assumption is very accurate for all of the studied gold chains even for rather long ones, as the differences between the phase-coherent calculations and the NEMD are small at sufficiently high temperatures. This implies that phononic heat transport is coherent and that the ballistic assumption is valid for those atomic-size systems.

The rest of this paper is organized as follows. In Sec. II, we briefly describe the newly developed computational method. We explain how we obtain the phononic thermal conductance with the help of nonequilibrium Green's function techniques and how the dynamical matrix is extracted from equilibrium MD. Furthermore, we recall in this section the basics of the classical NEMD approach, which we recently established [29] to take into account anharmonic effects in phonon heat flow. We conclude Sec. II by discussing further technical details of our MD simulations and by presenting some test calculations. Section III contains the main results of this work on the phononic heat conductance of Au single-atom contacts and chains, and in Sec. IV, we summarize our main findings.

## II. THEORETICAL METHODS

In this section, we describe in detail the two main transport methods that we employ later on to compute the phononic thermal conductance of atomic-scale metallic wires. We first discuss the novel coherent transport method that is based on the determination of the dynamical matrix from classical MD simulations in thermal equilibrium. Then, we briefly review the NEMD procedure that we have recently established to study phonon transport, taking into account anharmonic effects. Finally, we conclude this section by presenting technical details of our MD simulations and some simple test calculations.

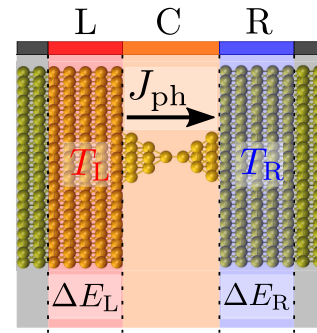


FIG. 1. Typical geometry of a metallic atomic-size contact studied in this work. The contact is divided into three regions, namely the central scattering region (C, orange), the left reservoir (L, red) and the right reservoir (R, blue). In this example, the contact consists of 1784 atoms in total, with 20 atoms located in the central part. On the left and right sides, two layers of fixed atoms (dark gray) stabilize the system during MD simulations. In the coherent transport description, the temperatures  $T_L$  and  $T_R$  differ infinitesimally, and no inherent heat current occurs in the equilibrium MD runs. In NEMD with  $T_L > T_R$ , the phononic heat current  $J_{ph}$  flows from the hot reservoir on the left at  $T_L$  to the cold reservoir on the right at  $T_R$ . Energies added or subtracted to maintain a constant temperature gradient are denoted by  $\Delta E_L$  and  $\Delta E_R$ .

### A. Equilibrium molecular dynamics and phase-coherent phonon heat transport

Let us start by describing, how the phononic heat conductance can be determined in the harmonic approximation and in the phase-coherent transport regime, where all the scattering events are elastic. Our goal is to compute the heat conductance due to the transport of phonons in a nanocontact, as the one depicted in Fig. 1.

Within the Landauer-Büttiker approach for coherent transport the phononic heat conductance in the linear response regime is given by [9,31]

$$\kappa_{ph} = \frac{1}{h} \int_0^\infty dE E \tau_{ph}(E) \frac{\partial n(E, T)}{\partial T}, \quad (1)$$

where  $\tau_{ph}(E)$  is the energy-dependent phononic transmission function,  $T$  is the temperature, and  $n(E, T) = [\exp(E/k_B T) - 1]^{-1}$  is the Bose function. To compute the transmission  $\tau_{ph}(E)$ , we use standard nonequilibrium Green's function techniques [9,31]. The basic ingredient is the dynamical matrix  $\underline{D}$ , which we assume to be given. Its determination is discussed further below, and it is typically the most time-demanding computational step.

We start by dividing the atomic contact into three regions, as shown in Fig. 1: the left (L) and right (R) reservoirs, which are semi-infinite, and the central (C) part. Following this division, the dynamical matrix can be written as

$$\underline{D} = \begin{pmatrix} \underline{D}_{LL} & \underline{D}_{LC} & \mathbf{0} \\ \underline{D}_{CL} & \underline{D}_{CC} & \underline{D}_{CR} \\ \mathbf{0} & \underline{D}_{RC} & \underline{D}_{RR} \end{pmatrix}, \quad (2)$$

where we assume that the reservoirs are not directly coupled. This latter assumption can typically be satisfied, by choosing the C region long enough. As discussed in Refs. [9,31], the phonon transmission function can be expressed in terms of

the phonon Green's function  $\underline{G}(E)$  as follows:

$$\tau_{\text{ph}}(E) = \text{Tr}[\underline{G}_{\text{CC}}(E)\underline{\Lambda}_{\text{L}}(E)\underline{G}_{\text{CC}}^\dagger(E)\underline{\Lambda}_{\text{R}}(E)]. \quad (3)$$

Here, the retarded phonon Green's function of the C part is given by

$$\underline{G}_{\text{CC}}(E) = [(E + i\eta)^2\mathbb{1} - \underline{D}_{\text{CC}} - \underline{\Sigma}_{\text{L}}(E) - \underline{\Sigma}_{\text{R}}(E)]^{-1}, \quad (4)$$

the embedding lead self-energies are

$$\underline{\Sigma}_Y(E) = \underline{D}_{\text{CY}}\underline{g}_{\text{YY}}(E)\underline{D}_{\text{YC}}, \quad (5)$$

and  $\underline{g}_{\text{YY}}(E)$  is the retarded surface Green's function of the reservoir  $Y = \text{L, R}$ . Finally, the broadening matrices  $\underline{\Lambda}_Y(E)$ , appearing in Eq. (3), are related to the self-energies via

$$\underline{\Lambda}_Y(E) = i[\underline{\Sigma}_Y(E) - \underline{\Sigma}_Y^\dagger(E)]. \quad (6)$$

The total transmission  $\tau_{\text{ph}}(E)$  can be decomposed at each energy  $E$  into contributions stemming from individual phonon transmission eigenchannels, in analogy to the electronic description [9,32], as

$$\tau_{\text{ph}}(E) = \text{Tr}[\underline{t}_{\text{ph}}(E)\underline{t}_{\text{ph}}^\dagger(E)] = \sum_i \tau_{\text{ph},i}(E), \quad (7)$$

where

$$\underline{t}_{\text{ph}}(E) = \underline{\Lambda}_{\text{R}}^{1/2}(E)\underline{G}_{\text{CC}}(E)\underline{\Lambda}_{\text{L}}^{1/2}(E) \quad (8)$$

is the transmission amplitude matrix and  $\tau_{\text{ph},i}(E)$  are the corresponding eigenvalues of the transmission probability matrix  $\underline{t}_{\text{ph}}(E)\underline{t}_{\text{ph}}^\dagger(E)$ .

With the knowledge of the dynamical matrix  $\underline{D}$  we can thus compute the phononic heat conductance  $\kappa_{\text{ph}}$  in the phase-coherent approximation. We now describe, how we obtain the dynamical matrix of a mechanical system by making use of classical MD in thermal equilibrium, assuming a harmonic model for the lattice vibrations [33].

We consider an infinite crystal in three spatial dimensions, where every atom  $i$  is located at its equilibrium position  $\mathbf{r}_i$ . The corresponding displacement of the atom  $i$  from the equilibrium position is specified by the vector  $\mathbf{u}_i$ . If the displacement is small for all atoms, we can use the harmonic approximation and describe the potential energy of the crystal as follows

$$U = \frac{1}{2} \sum_{i\alpha,j\beta} \left( \frac{\partial^2 U}{\partial u_{i\alpha} \partial u_{j\beta}} \right)_0 u_{i\alpha} u_{j\beta}. \quad (9)$$

Here  $\alpha, \beta = x, y, z$  indicate the spatial direction, and the subscript 0 reminds us that the derivatives are evaluated at the equilibrium positions of the atoms  $i, j$ . For convenience, we introduce the following notation for the second derivatives of the potential:

$$\Phi_{i\alpha,j\beta} = \left( \frac{\partial^2 U}{\partial u_{i\alpha} \partial u_{j\beta}} \right)_0, \quad (10)$$

which are the atomic force constants. As usual, and due to the translational symmetry of a crystal, the diagonal elements ( $i = j$ ) in the previous equation can be related to the off-diagonal elements ( $i \neq j$ ) by the so-called acoustic sum

rule

$$\Phi_{i\alpha,i\beta} = - \sum_{j \neq i} \Phi_{i\alpha,j\beta}. \quad (11)$$

The equation of motion of the atoms in this harmonic model reads

$$m_i \ddot{\mathbf{u}}_{i\alpha} = - \sum_{j,\beta} \Phi_{i\alpha,j\beta} \mathbf{u}_{j\beta}. \quad (12)$$

This relation has wavelike solutions of the form

$$\mathbf{u}_{i\alpha}(\mathbf{r}, t) = \frac{1}{\sqrt{m_i}} A_{i\alpha} e^{i(\mathbf{q}\cdot\mathbf{r} - \omega t)}, \quad (13)$$

where  $A_{i\alpha}$  is the amplitude and  $\mathbf{q}$  the wave vector. Introducing this ansatz into Eq. (12), we arrive at the secular equation

$$\underline{D} - \omega^2 \mathbb{1} = 0, \quad (14)$$

where

$$D_{i\alpha,j\beta} = \frac{1}{\sqrt{m_i m_j}} \Phi_{i\alpha,j\beta} \quad (15)$$

are the elements of the dynamical matrix and  $m_i$  is the mass of atom  $i$ .

For the calculation of the dynamical matrix, we follow Refs. [34–36] and compute it by monitoring the displacement of the atoms in classical equilibrium MD simulations. In simple terms the central idea of this method can be understood as follows. Let us consider a single particle attached to a massless spring with spring constant  $k$  and moving in one dimension along the  $x$  axis. The equipartition theorem relates the particle's elastic energy to the temperature  $T$  as follows:

$$\frac{1}{2} k \langle u_x^2 \rangle = \frac{1}{2} m \langle v_x^2 \rangle = \frac{1}{2} k_B T, \quad (16)$$

which implies that

$$k = \frac{k_B T}{\langle u_x^2 \rangle}. \quad (17)$$

Here,  $u_x$  characterizes the fluctuations of the particle relative to its equilibrium position,  $v_x$  is the velocity, and  $\langle \dots \rangle$  denotes an ensemble average. This relation suggests that force constants can be determined as the inverse of mean square displacements.

To establish this connection, we introduce the correlation matrix  $\underline{K}$  that describes the pairwise correlations between atomic displacements, defined as [34,36,37]

$$K_{i\alpha,j\beta} = \langle u_{i\alpha} u_{j\beta} \rangle = \langle r_{i\alpha} r_{j\beta} \rangle - \langle r_{i\alpha} \rangle \langle r_{j\beta} \rangle. \quad (18)$$

The dimension of the correlation matrix  $\underline{K}$  is  $3N \times 3N$ , if  $N$  is the number of atoms in the system. Following the idea above and thanks to the equipartition theorem, we relate the force constants to the spatial correlations in Eq. (18) as follows:

$$\Phi_{i\alpha,j\beta} = k_B T [\underline{K}^{-1}]_{i\alpha,j\beta}, \quad (19)$$

where  $[\underline{K}^{-1}]_{i\alpha,j\beta}$  denotes the element ( $i\alpha, j\beta$ ) of the inverse of the correlation matrix  $\underline{K}$ . Finally, the dynamical matrix is obtained from Eq. (15). Since  $\underline{D}$  is a thermodynamic quantity, it is affected by thermal noise in a finite sample. To take this into account, we introduce a cutoff  $r_c$  such that if  $|\mathbf{r}_i - \mathbf{r}_j| > r_c$ , then  $D_{i\alpha,j\beta} = 0$  for our nanocontacts.

In detail, we calculate interatomic force constants of nanojunctions, see Fig. 1, directly in real space rather than in reciprocal space. This is adequate, because the atomic junctions do not possess any periodicity. The procedure delivers the dynamical matrix in Eq. (2), however with finite regions L and R. To compute the phonon transmission, we retain only the parts  $\underline{D}_{CC}$ , describing the central part, and the couplings to L and R electrodes,  $\underline{D}_{CY} = \underline{D}_{YC}^\dagger$  with  $Y = L, R$ . To improve the description of the electrodes, we perform separate calculations for bulk gold. For this purpose, we employ periodic boundary conditions in three dimensions, construct the correlation matrix and subsequently the force constants in reciprocal space, as described in Refs. [34–36]. Through a Fourier transformation they are used to construct the semi-infinite electrodes in real space, effectively replacing the finite reservoir matrices  $\underline{D}_{LL}$  and  $\underline{D}_{RR}$  of the simulated nanojunctions with semi-infinite extended ones. It should however be noted that the electrodes enter only in terms of the electrode surface Green's functions in the calculation of the phononic transmission and derived thermal conductance. Therefore we compute electrode surface Green's functions with the help of the decimation technique from the bulk parameters [38]. The required length and minimal width of the surface region is determined by the couplings  $\underline{D}_{CY} = \underline{D}_{YC}^\dagger$  of the nanojunctions. The procedure follows the idea of the cluster-based approach to electronic quantum transport, described in Ref. [39], where the nanojunction, simulated in real space, is considered as the extended central cluster.

Thus we obtain the dynamical matrix from MD simulations at a certain temperature, by monitoring the positions of the atoms in time. This holds as long as the system under study is in thermal equilibrium, and the atoms fluctuate with small displacements around their equilibrium positions so that the harmonic approximation and equipartition theorem are valid. Since the molecular dynamics simulations, as we perform them here, are purely classical, the equipartition theorem holds down to the lowest temperatures. We can thus use Eqs. (18) and (19) to determine the dynamical matrix at any temperature and are in particular not limited to temperatures above the Debye temperature  $T_D$ . Let us finally stress that Refs. [34–36] calculate the correlation matrix and interatomic force constants in reciprocal space, as we do for the bulk parameters. However, the construction of the correlation and force constant matrices directly in real space, as we perform it here for the atomic junctions of the form visible in Fig. 1, has not been implemented before to the best of our knowledge.

In the following, we refer to the procedure of force constant determination through MD at a certain  $T$  and subsequent heat conductance calculations in the Landauer-Büttiker framework, using Eq. (1) at that same  $T$ , as MD@ $T$ -LB. An approximation along the lines of typical DFT approaches [40] is to compute the force constants at a single fixed temperature  $T_{\text{fix}}$ , but to nonetheless determine  $\kappa_{\text{ph}}$  at different  $T$  through Eq. (1). This assumes that force constants depend only weakly on temperature, and we refer to this simplified procedure as MD@ $T_{\text{fix}}$ -LB.

MD@ $T$ -LB and MD@ $T_{\text{fix}}$ -LB are both applicable to any system, where equilibrium MD simulations are available. The MD simulations can be based on empirical interatomic

interactions to largely accelerate computations, but also *ab initio* MD is possible.

## B. Nonequilibrium molecular dynamics and incoherent phonon heat transport

The method explained in the previous section describes phonon flow in the phase-coherent transport regime, where anharmonic effects are assumed to be small. To assess the impact of inelastic phonon-phonon interactions on the phononic heat conductance of metallic atomic-size contacts beyond a temperature-dependent renormalization of harmonic force constants, we employ a method that we have recently presented [29]. It is based on classical MD simulations under an applied temperature gradient, referred to as NEMD. We briefly describe it here, while details of the MD calculations are explained in the next section.

We consider an atomic contact, as depicted in Fig. 1, featuring a hot reservoir with temperature  $T_L$  and a cold reservoir with temperature  $T_R < T_L$ . A phononic heat current  $J_{\text{ph}}$  thus flows from left to right. Because we are only interested in the phonon transport through the central region, the atom dynamics of the reservoirs are of no direct importance. We therefore apply a strong rescale thermostat to both reservoirs. It rescales the velocities  $v_i$  of the atoms, following the equipartition theorem

$$\langle E_Y \rangle = \sum_{i=1}^{N_Y} \frac{1}{2} m_i \langle v_i^2 \rangle = \frac{3}{2} N_Y k_B T_Y, \quad (20)$$

where  $N_Y$  is the number of atoms in electrode  $Y$ . Rescaling to a target temperature  $T_{Y,t}$  corresponds to a change  $\Delta E_Y$  in energy of the thermostatted group of atoms

$$\Delta E_Y = \langle E_Y \rangle \left( 1 - \frac{T_{Y,t}}{T_Y} \right). \quad (21)$$

Heating therefore corresponds to a negative change in energy and cooling to a positive one. Following Fourier's law, the phonon thermal conductance  $\kappa_{\text{ph}}$  of the junction is given by

$$\kappa_{\text{ph}} = \frac{J_{\text{ph}}}{\Delta T} = \frac{1}{2\Delta t} \frac{-\Delta E_L + \Delta E_R}{T_L - T_R}. \quad (22)$$

Since the energy and temperature of the reservoirs fluctuate, we monitor  $\Delta E_Y$  and  $T_Y$  over a sufficient long time to reach reliable averages.

Using classical statistics, the NEMD method takes into account both elastic and inelastic effects in phonon transport. Therefore a comparison of this method with the phase-coherent one, described above, will allow us to determine the relevance of inelastic scattering in the phonon transport through atomic contacts. We note that the NEMD description is expected to break down at sufficiently low temperatures, when quantum statistics play a role. Roughly, we expect that  $T$  needs to be larger than the Debye temperature  $T_D$  for the classical approximation to hold. In comparison, the phase-coherent method in the harmonic approximation MD@ $T$ -LB, see Sec. II A, correctly incorporates Bose-Einstein quantum statistics through Eq. (1), once a dynamical matrix has been determined.

### C. Technical details of molecular dynamics simulations

The transport methods, described in the previous two sections, use classical MD simulations, either in equilibrium or nonequilibrium. In this section, we explain in detail how we carry out the simulations.

All the MD simulations presented in this work are performed with the open-source package LAMMPS [41,42]. We describe interatomic interactions with the embedded-atom method [43], taking the potential for Au from Ref. [44]. The use of the same interatomic interaction potential for MD@ $T$ -LB, MD@ $T_{\text{fix}}$ -LB, and NEMD ensures the comparability of the simulations. Junction geometries are oriented such that the  $\langle 111 \rangle$  crystallographic direction coincides with the transport direction. The central scattering region of the gold contacts consists of two adjacent pyramids, connected by a chain of atoms. To the left and right of the central part, see Fig. 1, semi-infinite reservoirs with 630 atoms are followed by two atomic layers of 252 atoms with fixed atoms. These outermost regions are used to stabilize the junctions during the simulations. For each junction geometry we did an energy minimization run for the C part, see Fig. 1, using the conjugate gradient method of LAMMPS prior to our MD simulations for force constant extraction. The reservoirs L and R are subsequently coupled to the optimized C part such that minimal pressure or stress is exerted on the studied junctions. Orthogonal to the transport direction we employ periodic boundary conditions to model extended surfaces of the reservoirs. The studied contacts with a variable number of chain atoms consist of around 1800 atoms in total. The length of the junctions varies from about 33 Å for the shortest contact up to 61 Å for the longest one, measured from the leftmost layer of reservoir L to the rightmost layer of reservoir R. The dimer contact geometry, shown in Fig. 1, exhibits a junction length of about 35 Å.

For statistical analysis we provide random initial velocities to the junction atoms in L, C, and R regions to obtain different time evolutions during the simulations. For each temperature and each geometry we perform 20 individual simulations and average over the computed thermal conductances in this set. Thermal equilibration is achieved by applying a Nosé-Hoover thermostat to all junction atoms over a sufficiently long time of 1 ns to reduce fluctuations in temperature. This is done for the equilibrium MD and the NEMD simulations, respectively. If not mentioned otherwise, we use a time step of 1 fs in the MD simulations.

Following Sec. II A, the extraction of atomic force constants for the individual nanojunction simulation in the coherent transport method is done in the NVE ensemble without a thermostat to avoid interactions with an external heat bath. After thermal equilibration of the system the ensemble average of Eq. (18) is taken over 200 000 atomic configurations or frames to construct the correlation matrix, from which the force constants are obtained via Eq. (19). The total simulation time for the individual junction in the set amounts to 20 ns, with a snapshot being taken every 0.1 ps to achieve a good sampling.

Beside the force constants of the C part of the nanocontact and the couplings to L and R electrodes, we need the force constants for the bulklike electrodes. For this purpose,

we simulate bulk Au, using a primitive unit cell and periodic boundary conditions with a  $k$  grid of  $16 \times 16 \times 16$ . Starting with randomized velocities, an equilibration is performed with a Nosé-Hoover thermostat for 1 ns, as for the nanojunctions. Subsequently, correlations are determined in reciprocal space every 1 ps during a total time interval of 20 ns for an MD run in an NVE ensemble. Through the time average of the correlations, force constants are computed, which are then transformed to real space through a Fourier transformation, where we impose the FCC space group symmetry, as described for the electronic case in Ref. [39]. Using the symmetrized bulk parameters in real space, electrode surface Green's functions are constructed, assuming transverse periodic boundary conditions of  $32 \times 32$  lattice constants.

To account for the thermal noise in our Landauer-Büttiker-based transport calculations, we find it necessary to choose a finite cutoff radius  $r_c$  for the atomic force constant determination of the nanocontacts, cf. Sec. II A. To find out, which spatial cutoff is reasonable, we systematically studied the phononic thermal conductance as a function of  $r_c$  for two junctions with chain lengths of 1, the monomer, and 8. The cutoff was varied from 2 to 52 Å at  $T = 300$  K. For the monomer the phononic thermal conductance is basically independent of the cutoff for  $6 \text{ Å} \leq r_c \leq 14 \text{ Å}$ , for the chain with a length of 8 atoms  $\kappa_{\text{ph}}$  is constant for  $6 \text{ Å} \leq r_c \leq 28 \text{ Å}$ . Therefore  $r_c = 10 \text{ Å}$  appears to be a reasonable choice for short as well as long chains.

The (targeted) temperature difference between the two reservoirs in the NEMD method is chosen as  $\Delta T = T_L - T_R = 30$  K. The temperature difference is established by steadily heating the reservoir L, see Fig. 1, with a slope of 30 K/ns up to the target temperature  $T_{L,t}$ , while the cold reservoir R is kept at  $T_{R,t}$ . The C part of the junction is simulated in the NVE ensemble without applying an external thermostat during this heating. After the heating process the two reservoirs L and R of the junction are once more equilibrated for 1 ns at their respective temperatures  $T_{L,t}$  and  $T_{R,t}$  to reduce temperature fluctuations. Given the steadily maintained temperature difference, the changes of energy  $\Delta E_Y$  and temperature  $T_Y$  in the electrode  $Y = L, R$  are determined over a sufficient long time of 200 ns in each individual junction simulation, with a snapshot taken every 1 ps to achieve a good sampling. For the calculation of the phononic thermal conductance value of a single run in the set of 20, we average over the last 50,000 data points. Note that we always specify phononic conductance values of the NEMD calculations with respect to the target temperature  $T_{R,t}$  of the cold reservoir.

Since we use a geometry, where the central part is directly coupled to two thermostatted electrodes, see Fig. 1, finite size effects need to be analyzed. Therefore we systematically added 3, 6, 12, 18, and 36 atom layers with the lateral size of those in L and R parts to the C part and studied the influence on the phononic thermal conductance. We found the thermal conductance to slightly increase with the size of the reservoirs, but the changes in  $\kappa_{\text{ph}}$  were only on the order of a few pW/K at 300 K. For this reason and for the sake of computational efficiency, we selected the contacts with the smallest number of atoms in the C region, as shown in Fig. 1.

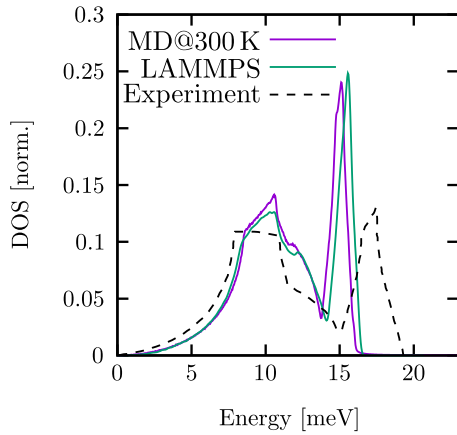


FIG. 2. Bulk phonon DOS, calculated at 300 K (solid purple line) with our approach, and experimental DOS (dashed black line) taken from Ref. [45] at 297 K. Additionally we show a DOS determined at 300 K with existing functionality of LAMMPS [35,36,42] (solid green line). DOS curves are normalized by the total area enclosed.

#### D. Test of the phase-coherent transport method

To test the accuracy of the phase-coherent transport method MD@ $T$ -LB, we first assess the quality of the bulk description. For this purpose we extracted bulk force constants in reciprocal space, as described in Secs. II A and II C, and compare the computed density of states (DOS) with available experimental data [45]. As it is visible in Fig. 2, the agreement is satisfactory. The main difference is that the theory underestimates the energy of the vibrational modes at the second peak of the DOS by about 20%. The good agreement of our calculation with the DOS, computed with LAMMPS directly [35,36,42], illustrates that deviations between theory and experiment originate from the employed potential itself.

As another analytically trackable test case we consider a one-dimensional (1D) atomic chain. Employing MD within the NVE ensemble, we simulated a chain containing 16 atoms, assuming periodic boundary conditions, a mass of  $m$  per atom, harmonic bonds with interatomic potentials  $U = \frac{1}{2}k(r - r_0)^2$  and the spring constant  $k$ , see the inset of Fig. 3. The equilibrium bond distance in the chain was set to  $r_0$ . Using a time step of  $5 \times 10^{-3} \sqrt{m/k}$  in the MD simulations, the equilibration employed a Langevin thermostat at a temperature of  $T = 5 \times 10^{-3} kr_0^2/k_B$  for  $5 \times 10^6$  steps. Correlations were recorded regularly every 250 steps for a total of  $2 \times 10^7$  steps, from which we obtain the force constants and dynamical matrix. Note that we specify all physical quantities of this model in terms of reduced units of  $r_0$ ,  $m$ ,  $k$  and  $k_B$ . The 1D chain was divided into L, C and R parts, as shown in Fig. 3, with the C part containing  $N_C = 6$  atoms. The phononic transmission  $\tau_{\text{ph}}(E)$  was then determined within the nonequilibrium Green's function formalism, as described in Sec. II A, using the analytic solution for the surface Green's function of a semi-infinite chain with phononic nearest neighbor couplings  $k$ . As it is evident from Fig. 3, our results compare in an excellent manner to the fully analytical solution that can be obtained for this simple model. The agreement holds in the whole range of energies studied, and especially the edge at  $2\sqrt{k/m}$  is reproduced very accurately.

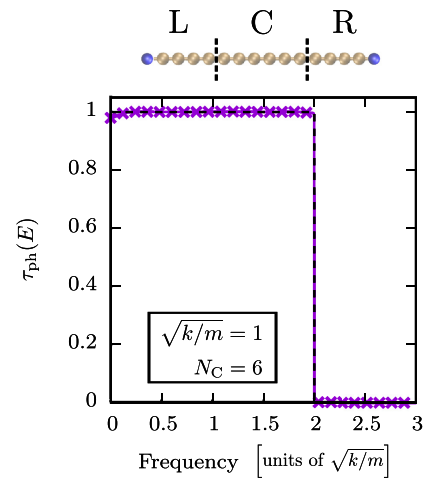


FIG. 3. Phononic transmission function  $\tau_{\text{ph}}(E)$  of a 1D chain with harmonic bonds. We compare the curve computed with force constants extracted from MD simulations (solid purple line and purple crosses) to the expected analytical behavior (dashed black line). The different quantities are given in reduced units. Above the plot we show the system under study, indicating L, C and R regions. The blue-colored atoms are neighbors due to the assumed 1D periodic boundary conditions.

### III. RESULTS

In this section, we present the main results of this work. We analyze quasi-1D Au chains coupled to three-dimensional electrodes and discuss the influence of temperature and chain length on the phononic heat conductance. In addition, we compare phase-coherent transport to the NEMD method, which includes also inelastic effects from anharmonic phononic interactions.

#### A. Length dependence of the phonon thermal conductance of Au chains

The main strength of our phase-coherent transport method MD@ $T$ -LB is the inherent temperature dependence that MD simulations take into account and the time-efficient description even of large systems of several thousand atoms, if empirical interatomic interactions are used. We will demonstrate these aspects in this section by applying MD@ $T$ -LB and MD@ $T_{\text{fix}}$ -LB to quasi-1D Au chains. To analyze the importance of inelastic scattering events for the phononic thermal conductance, we consider different lengths of the central chain of the junction by varying atom numbers from 1 to 12. We will compare the predictions of the three different methods, introduced in Sec. II: (i) the phase-coherent method MD@ $T$ -LB, (ii) MD@ $T_{\text{fix}}$ -LB with  $T_{\text{fix}} = 100$  K, and (iii) classical NEMD. Method (ii) assumes that atomic force constants are basically independent of temperature and correspond to those at 100 K. It is comparable to a static DFT ansatz, where force constants are for instance evaluated once with density functional perturbation theory for the ground state geometry [27,32].

Figure 4 shows the phononic thermal conductance as a function of temperature for the different computational methods. Going from the top left to the bottom right, the length

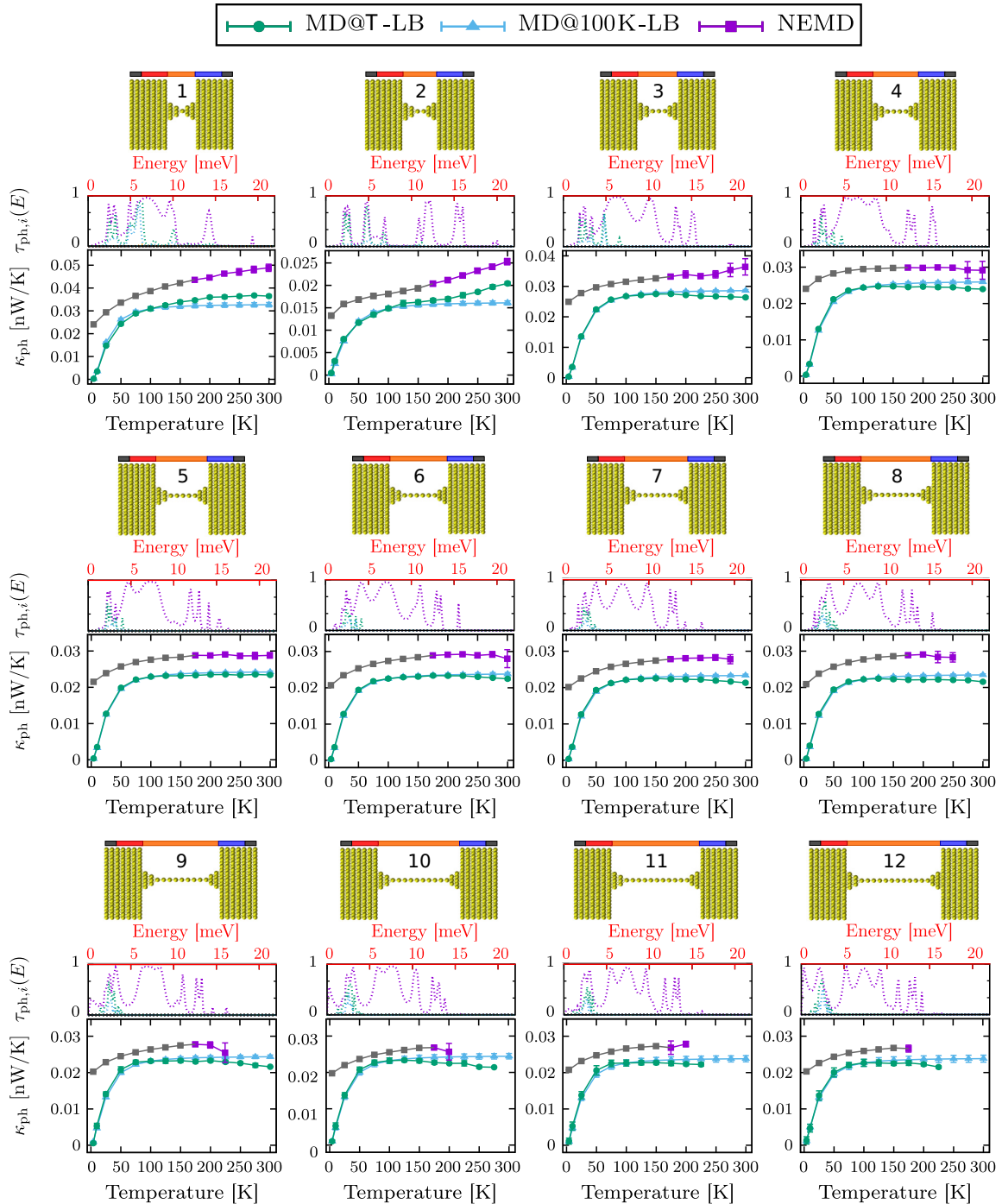


FIG. 4. Phonon thermal transport through gold junctions. Junction geometries are shown in the top panels. The length of the central atomic chain ranges from 1 (top left) to 12 atoms (bottom right) between the two pyramids. Middle panels show phonon eigenchannel transmissions  $\tau_{ph,i}(E)$  with force constants determined at 100 K. Phononic thermal conductance  $\kappa_{ph}$ , bottom panels, as a function of temperature for the three studied methods: We compare the results of the coherent method MD@T-LB (green circles), a simplified coherent method with a temperature-independent approximation for the dynamical matrix MD@100K-LB (blue triangles), and classical NEMD (purple squares). Mean values solely consider junctions that did not break during the 20 simulations performed at each  $T$  in MD@T-LB and NEMD, and error bars specify standard deviations in this set of thermal conductances. For MD@100K-LB predictions of  $\kappa_{ph}$  are made at each  $T$  using the force constants determined in different simulation runs at  $T_{fix} = 100$  K, and error bars visualize the corresponding standard deviations. Since NEMD is based on a classical theory, its results at sufficiently low temperatures are not meaningful. To visualize this, we grayed out data points for  $T < T_D \approx 170$  K.

of the central chain increases. Junction geometries are displayed in the top panels of Fig. 4, middle panels show the transmissions of phonon eigenchannels as a function of energy for the phase-coherent calculation using force constants extracted at 100 K, and bottom panels depict phononic thermal conductances as a function of temperature. Values of  $\kappa_{\text{ph}}$  represent averages over the 20 simulations performed in MD@ $T$ -LB and NEMD for each nanocontact at a fixed  $T$ , while error bars characterize the standard deviation. The averages solely consider junctions that did not break during the simulation runs. Since we find breakage especially for longer chains at elevated temperatures, the sample size for some data points is less than 20. For example, for the junction with 12 chain atoms, every NEMD run at or above a temperature of 200 K broke before the end of the simulation time, and hence no data is available at  $T \geq 200$  K for this method. Similar statements hold for MD@ $T$ -LB, but we generally find that the metallic atomic contacts break at lower temperatures in NEMD than in equilibrium MD. Since we specify the temperature in NEMD with regard to the colder reservoir  $T_{\text{R,t}}$ , the applied temperature gradient leads to a higher effective temperature of the nanostructures in NEMD than in equilibrium MD. This rationalizes the reduced stability observed in the NEMD simulations. Since junctions are generally stable at  $T = 100$  K, MD@100K-LB yields data points throughout the entire temperature range studied. The standard deviations for MD@100K-LB characterize differences in predicted  $\kappa_{\text{ph}}$  values, resulting from the force constants determined in the 20 simulation runs at 100 K.

Concerning phonon transmission, Fig. 4 shows that for all junctions only up to three transmission eigenchannels contribute. While the three channels may exhibit a similar transmission for energies  $E \lesssim 7$  meV, a single channel determines the transmission above. For short chains, second and third channels range up to energies of 10 meV but tend to vanish sooner for long chains. In general, a transmission eigenchannel at a fixed energy is a linear combination of many different local vibrations [32]. In the case of the studied chain junctions, the narrowest part of the wire is one-atom thick and can be assumed to be quasi 1D. In that limit the transmission eigenchannels should reflect the three acoustic phonon modes of a 1D chain, i.e., one longitudinal and two transversal [27,32]. This behavior is confirmed by our results, see the middle panels of Fig. 4, and conveys that we are basically dealing with quasi-1D phonon transport.

Let us justify the choice of  $T_{\text{fix}} = 100$  K in MD@ $T_{\text{fix}}$ -LB for the approximation of the thermal conductance with temperature-independent force constants. MD@ $T$ -LB in Fig. 4 shows that the thermal conductance is well saturated at this temperature, particularly for long chains. Hence,  $T_{\text{fix}} = 100$  K allows us to identify crucial temperature-dependent changes in force constants by comparison of MD@ $T$ -LB and MD@100K-LB. Results of classical NEMD are only valid at high enough temperatures  $T \gtrsim T_{\text{D}}$ . Above the Debye temperature  $T_{\text{D}}$ , the statistics of phonons are basically classical and quantum corrections can thus be neglected. For sufficiently low temperatures  $T \ll T_{\text{D}}$ , NEMD cannot predict the correct temperature dependence of the phononic thermal conductance. To signal caution, we have hence grayed out NEMD results for  $T < T_{\text{D}} \approx 170$  K in Fig. 4.

The thermal conductance predicted by MD@ $T$ -LB increases rather monotonically with  $T$  in Fig. 4 for the short chains, especially the monomer and dimer, while we typically observe a saturation for longer chain lengths and subsequent weak decay. For the monomer and dimer,  $\kappa_{\text{ph}}$  of MD@ $T$ -LB is larger for  $T > 100$  K compared to the values predicted with MD@100K-LB. This signals a significant dependence of force constants on temperature. Indeed, we assign the increase of the thermal conductance for short chain lengths and high temperatures to the thermal expansion of electrode reservoirs. Since we use fixed atoms to the left and right side, reservoirs can only expand towards the center of the junctions, narrowing the gap distance between left and right electrode surfaces. This decreases the mean spatial distance between the atoms in the central scattering region and thus enhances the phononic thermal conductance. For longer chains, starting with the trimer, MD@ $T$ -LB and MD@100K-LB give very comparable results. Indeed the heat conductance predicted by MD@100K-LB overestimates those of MD@ $T$ -LB, which slightly decays at high enough  $T \gtrsim 150$  K. We assign this effect to disordered chains, which form due to the thermal expansion of the electrode reservoirs. If we monitor the mean displacement of the chain atoms transverse to the transport direction, the chains are less linear at higher temperature, increasing the elastic scattering and thus lowering the overall phononic transmission. In that sense, in MD@ $T$ -LB the temperature affects the properties of the phonon modes and subsequently the energy dependent phononic transmission as the geometry of the nanojunctions changes. We note that for MD@100K-LB, using a temperature-independent dynamical matrix determined at  $T_{\text{fix}} = 100$  K, the phononic transmission is temperature independent and the phonon thermal conductances in Fig. 4 hence saturate at a constant value with increasing  $T$ . The small deviations in  $\kappa_{\text{ph}}$  of a few pW/K between MD@ $T$ -LB and MD@100K-LB methods show that a temperature-independent description of atomic force constants is generally a good approximation for the studied systems. Differences between MD@ $T$ -LB and MD@100K-LB may be used to learn more about the mechanical and thermal characteristics of a nanostructure.

The heat conductance determined with NEMD in Fig. 4 is always larger than those of MD@ $T$ -LB. Quantitatively, within the limits of applicability of classical statistics, i.e.  $T \gtrsim T_{\text{D}}$ , deviations are relatively small and at most of the order of 10 pW/K. The qualitative behavior agrees very well, i.e.,  $\kappa_{\text{ph}}$  increases rather monotonically with  $T$  for short chains, including the monomer, dimer and additionally the trimer, while we observe a saturation for longer chain lengths and a slight decay. The suppression of the heat conductance in NEMD for long chain lengths and high  $T$  could in principle be assigned both to the effect of increased elastic scattering due to induced chain disorder by thermal reservoir expansion and increased inelastic scattering due to phonon-phonon interactions [46]. However, the quantitatively similar trends of the phase-coherent method MD@ $T$ -LB suggest that the slight suppression of  $\kappa_{\text{ph}}$  at high  $T$  originates from elastic scattering in an effectively disordered chain.

Overall, the agreement of results of the classical NEMD and the temperature-dependent, coherent method MD@ $T$ -LB in Fig. 4 is very good. We note that we are comparing two



methods that are making completely different assumptions about the theoretical description of phononic heat transport. Let us also emphasize that our computational results are statistically very stable, as can be seen by the small error bars. Absolute differences are only about a few pW/K, and we observe that differences between NEMD and MD@ $T$ -LB tend to decrease with increasing chain length. While we use large nanocontacts and a high sample size in our calculations, differences may still arise from systematic numerical uncertainties of our finite-size study.

The phononic thermal conductance of single-atom contacts has already been studied and discussed intensively in other works using DFT-based methods [4,27,28]. In Ref. [4], phononic thermal transport was found to yield only about 4% of the total thermal conductance  $\kappa = \kappa_{el} + \kappa_{ph}$  at room-temperature for a gold dimer junction. With a prevalent electronic contribution of  $\kappa_{el} \approx 0.59$  nW/K this corresponds to a phononic thermal conductance of about  $\kappa_{ph} \approx 0.025$  nW/K at  $T = 300$  K. Our results predict a phononic thermal conductance of  $\kappa_{ph} = 0.020$  nW/K at  $T = 300$  K for the studied gold dimer junction in Fig. 4 using the MD@ $T$ -LB approach, which is in excellent agreement with the one calculated via DFT [4]. Another DFT-based calculation of a gold dimer was presented in Ref. [27], where the validity of the Wiedemann-Franz law was investigated for metallic atomic-size contacts. In that case Klöckner *et al.* determined a phononic thermal conductance of  $\kappa_{ph} = 0.051$  nW/K at room temperature, which is about 2.5 times higher than our result in this work. In both reports [4,27], the geometry of the studied dimer junction slightly differs from the one that we are using here. However, these comparisons show that our MD@ $T$ -LB approach is a valid description of phononic thermal transport.

To get a more detailed view on the length dependence of the thermal conductance, we show it as a function of the number of atoms in the central chain of the junction for selected temperatures in Fig. 5. Results of the three studied methods are compiled in separate panels. In every case, we see finite-size oscillations and a decline of  $\kappa_{ph}$  with increasing chain length. For larger chain lengths,  $\kappa_{ph}$  is rather constant and shows only weak oscillations, a clear signature of ballistic conduction. For all three methods, the thermal conductance is suppressed at a chain length of two atoms. This reduction of the thermal conductance can be traced back to a suppression of the phonon transmission of the dominant transmission eigenchannel in the energy range between 5 and 10 meV, see the panels containing the phononic transmission coefficients in Fig. 4. Whether this effect is real or an artifact of the employed embedded-atom method potential is unclear, however, and remains as an interesting point for experimental examination. The plots for MD@ $T$ -LB and MD@100K-LB also show that above about 100 K the thermal conductance depends only weakly on temperature. For the thermal conductance of the classical NEMD calculations in the bottom panel of Fig. 5, we notice only a weak temperature dependence. Consistent with Fig. 4, the thermal conductance at  $T = 25$  K is very similar to those at  $T = 100$  K. This erroneous prediction arises from classical statistics and differs from MD@ $T$ -LB and MD@100K-LB, which both properly take Bose-Einstein quantum statistics into account. We note that some data points are missing from MD@ $T$ -LB and NEMD, since junctions

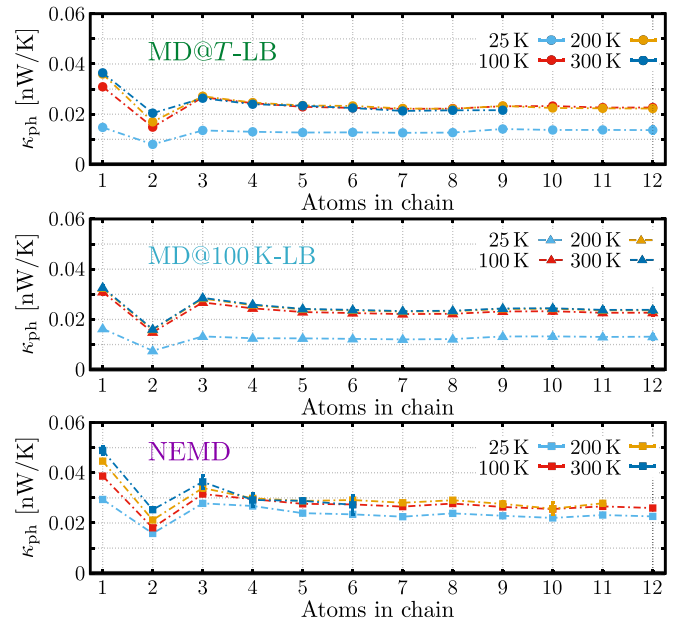


FIG. 5. Thermal conductance  $\kappa_{ph}$  as a function of the number of atoms in the chain at temperatures of 25, 100, 200, and 300 K. The results of the three different methods are shown separately, namely for MD@ $T$ -LB, MD@100K-LB and NEMD, going from top to bottom.

with long atomic chains tend to break at elevated temperatures, as already discussed in the context of Fig. 4.

DFT-based calculations of atomic junctions of Au for chain lengths ranging from two to five atoms by Bürkle and Asai [28] show that the ratio  $\kappa_{ph}/\kappa_{el}$  between phononic and electronic thermal conductance at room-temperature depends only weakly on the length of the junction. Apart perhaps from the data point of the dimer, this is consistent with the results of Fig. 5 in the sense that the phononic thermal conductance is almost independent of the chain length.

To summarize, for  $T \gtrsim T_D$  the results of the three different calculation methods differ only by a few pW/K for Au metallic atomic contacts containing long chains. This strongly suggests that the phononic thermal transport through the studied junctions is phase-coherent even for rather long chains with up to 12 atoms. Longer chains could not be studied here for practical reasons, since most of them broke during simulations. While it would be interesting to investigate much longer chains to see if there is a critical length above which scattering is no longer elastic, experiments indicate that a maximum length of up to eight chain atoms can be realized [47–49]. Altogether our results corroborate that the harmonic approximation used in the coherent transport calculations is well suited for the studied atomic-size junctions.

## B. Computational costs

To evaluate the efficiency of the newly introduced phase-coherent phonon transport methods MD@ $T$ -LB and MD@ $T_{fix}$ -LB, let us now compare the computational costs of the presented simulation procedures. We do this exemplarily for the monomer junction shown in the upper leftmost panel of Fig. 4. The junction consists of 1783 atoms.

At a fixed temperature we need about 288 core-h for one NEMD run, including the MD simulation and calculation of the phononic thermal conductance. With a total number of 20 individual runs per temperature to construct a sufficient statistical data base and 14 different temperatures, this value needs to be multiplied by a factor of 280 to obtain the total amount of core-h. The study of a single junction type using NEMD, as shown for  $\kappa_{\text{ph}}$  in the upper leftmost panel of Fig. 4, thus corresponds to a computational cost of about 80,640 core-h.

In the phase-coherent regime, using MD@ $T$ -LB, the calculation of the phononic thermal conductance takes about 48 core-h. This includes 28 core-h for the equilibrium MD simulation and additional 20 core-h for the calculation of force constants and transport. With the same statistical sample of 20 individual simulations per temperature and 14 different studied temperatures, this results in a total computational cost of about 13,440 core-h. This is about 6 times faster than NEMD. If we only compare the MD part of the calculations, the coherent description is about 10 times faster than NEMD.

If we disregard the temperature dependence of the interatomic force constants and use the simplified MD@ $T_{\text{fix}}$ -LB procedure for the evaluation of phase-coherent phononic conduction, a single geometry can be studied even more efficiently. As for MD@ $T$ -LB, the total computational cost of a single transport calculation at  $T_{\text{fix}} = 100$  K equals to about 48 core-h. With 20 individual simulations at this temperature for statistical relevance, this yields about 960 core-h for a single junction geometry. Note that the transport calculations at the remaining 13 different temperatures correspond to negligible computational demand, which we neglect here. Hence, MD@ $T_{\text{fix}}$ -LB requires about a factor 14 less core-h as compared to MD@ $T$ -LB and a factor of 84 as compared to NEMD. Considering that results of MD@ $T$ -LB and MD@ $T_{\text{fix}}$ -LB differ little for the metallic atomic contacts and in relation to the computational costs, this approximation can certainly be used to obtain an excellent first guess.

#### IV. CONCLUSIONS

In this work, we have introduced a method to calculate atomic force constants of nanostructures directly from MD simulations in thermal equilibrium by tracking atomic positions in real space. The force constants are then used to evaluate the phononic contribution to the thermal conductance of nanocontacts. This step utilizes the framework of the Landauer-Büttiker scattering theory for coherent transport, expressed in terms of nonequilibrium Green's function techniques. At the example of monoatomic metallic nanocontacts, we have confirmed the validity and accuracy of this novel approach.

The advantage of the new coherent transport method is twofold. On the one hand, if reliable semiempirical interatomic interaction potentials are available, it is less time-consuming than *ab initio* approaches, which facilitates the modeling of large systems. We have illustrated this fact by showing calculations for junctions with up to 1794 atoms, which are difficult to handle with conventional DFT-based methods. On the other hand, our MD-based approach automatically takes into account the temperature dependence of the dynamical matrix, which is usually ignored in static *ab initio* procedures.

For gold metallic nanowires, featuring lengths of atomic chains from 1 to 12 atoms, we have assessed the relevance of inelastic effects due to anharmonic phonon-phonon scattering by comparing results of the phase-coherent method to those obtained with classical NEMD. While being applicable only above the Debye temperature  $T_D$  because of classical statistics, the latter approach naturally takes inelastic effects into account. At sufficiently high temperatures ( $T \gtrsim T_D$ ), where all relevant phonon modes are populated, the phononic heat conductance is only weakly dependent on temperature and chain length. Overall this behavior, which we observed consistently for the MD@ $T$ -LB as well as the NEMD description, clearly signals the ballistic nature of phonon conduction in the studied metallic atomic-size contacts. Thus we conclude that the nanojunctions are sufficiently stiff to suppress anharmonic phonon interactions, leading to mainly elastic scattering and phase-coherent phonon heat transport.

To conclude, we emphasize that the coherent transport method MD@ $T$ -LB, introduced in this work, is by no means restricted to metallic atomic-size contacts: it can be applied to describe the coherent phonon transport in any nanostructure, if MD simulations can be carried out. In this sense, we anticipate that this method may become very useful to investigate different questions related to heat flow through molecular junctions [6,7], where the thermal conductance is determined by phonon conduction.

#### ACKNOWLEDGMENTS

We thank J. C. Klöckner for many stimulating discussions. P.N. and F.P. were funded by the Collaborative Research Center (SFB) 767 of the German Research Foundation (DFG). J.C.C. thanks the Spanish Ministry of Science and Innovation (Grant No. PID2020-114880GB-I00) for financial support as well as the DFG and SFB 767 for sponsoring his stay at the University of Konstanz as a Mercator Fellow. F.M. and P.N. gratefully acknowledge the Gauss Centre for Supercomputing e.V. for providing computing time through the John von Neumann Institute for Computing (NIC) on the Supercomputer JUWELS at the Jülich Supercomputing Centre (JSC). Furthermore, the authors acknowledge support by the state of Baden-Württemberg through the bwHPC initiative.

[1] E. Pop, Energy dissipation and transport in nanoscale devices, *Nano Res.* **3**, 147 (2010).

[2] D. G. Cahill, P. V. Braun, G. Chen, D. R. Clarke, S. Fan, K. E. Goodson, P. Keblinski, W. P. King, G. D. Mahan, A. Majumdar,

- H. J. Maris, S. R. Phillpot, E. Pop, and L. Shi, Nanoscale thermal transport. II. 2003-2012, *Appl. Phys. Rev.* **1**, 011305 (2014).
- [3] A. J. Minnich, Advances in the measurement and computation of thermal phonon transport properties, *J. Phys.: Condens. Matter* **27**, 053202 (2015).
- [4] L. Cui, W. Jeong, S. Hur, M. Matt, J. C. Klöckner, F. Pauly, P. Nielaba, J. C. Cuevas, E. Meyhofer, and P. Reddy, Quantized thermal transport in single-atom junctions, *Science* **355**, 1192 (2017).
- [5] N. Mosso, U. Drechsler, F. Menges, P. Nirmalraj, S. Karg, H. Riel, and B. Gotsmann, Heat transport through atomic contacts, *Nat. Nanotechnol.* **12**, 430 (2017).
- [6] L. Cui, S. Hur, Z. A. Akbar, J. C. Klöckner, W. Jeong, F. Pauly, and S.-Y. Jang, Thermal conductance of single-molecule junctions, *Nature (London)* **572**, 628 (2019).
- [7] N. Mosso, H. Sadeghi, A. Gemma, S. Sangtarash, U. Drechsler, C. Lambert, and B. Gotsmann, Thermal Transport through Single-Molecule Junctions, *Nano Lett.* **19**, 7614 (2019).
- [8] N. Agraït, A. L. Yeyati, and J. M. van Ruitenbeek, Quantum properties of atomic-sized conductors, *Phys. Rep.* **377**, 81 (2003).
- [9] J. C. Cuevas and E. Scheer, *Molecular Electronics: An Introduction to Theory and Experiment*, 2nd ed. (World Scientific, Singapore, 2017).
- [10] J. M. Krans, J. M. van Ruitenbeek, V. V. Fisun, I. K. Yanson, and L. J. de Jongh, The signature of conductance quantization in metallic point contacts, *Nature (London)* **375**, 767 (1995).
- [11] E. Scheer, N. Agraït, J. C. Cuevas, A. L. Yeyati, B. Ludoph, A. Martín-Rodero, G. R. Bollinger, J. M. van Ruitenbeek, and C. Urbina, The signature of chemical valence in the electrical conduction through a single-atom contact, *Nature (London)* **394**, 154 (1998).
- [12] H. E. van den Brom and J. M. van Ruitenbeek, Quantum Suppression of Shot Noise in Atom-Size Metallic Contacts, *Phys. Rev. Lett.* **82**, 1526 (1999).
- [13] P. J. Wheeler, J. N. Russom, K. Evans, N. S. King, and D. Natelson, Shot noise suppression at room temperature in atomic-scale Au junctions, *Nano Lett.* **10**, 1287 (2010).
- [14] R. Chen, P. J. Wheeler, and D. Natelson, Excess noise in STM-style break junctions at room temperature, *Phys. Rev. B* **85**, 235455 (2012).
- [15] R. Vardimon, M. Matt, P. Nielaba, J. C. Cuevas, and O. Tal, Orbital origin of the electrical conduction in ferromagnetic atomic-size contacts: Insights from shot noise measurements and theoretical simulations, *Phys. Rev. B* **93**, 085439 (2016).
- [16] D. C. Guhr, D. Rettinger, J. Boneberg, A. Erbe, P. Leiderer, and E. Scheer, Influence of Laser Light on Electronic Transport through Atomic-Size Contacts, *Phys. Rev. Lett.* **99**, 086801 (2007).
- [17] J. K. Viljas and J. C. Cuevas, Role of electronic structure in photoassisted transport through atomic-sized contacts, *Phys. Rev. B* **75**, 075406 (2007).
- [18] N. Ittah, G. Noy, I. Yutsis, and Y. Selzer, Measurement of electronic transport through  $1G_0$  gold contacts under laser irradiation, *Nano Lett.* **9**, 1615 (2009).
- [19] D. R. Ward, F. Hüser, F. Pauly, J. C. Cuevas, and D. Natelson, Optical rectification and field enhancement in a plasmonic nanogap, *Nat. Nanotechnol.* **5**, 732 (2010).
- [20] B. Ludoph and J. M. van Ruitenbeek, Thermopower of atomic-size metallic contacts, *Phys. Rev. B* **59**, 12290 (1999).
- [21] M. Tsutsui, T. Morikawa, A. Arima, and M. Taniguchi, Thermoelectricity in atom-sized junctions at room temperatures, *Sci. Rep.* **3**, 3326 (2013).
- [22] C. Evangeli, M. Matt, L. Rincón-García, F. Pauly, P. Nielaba, G. Rubio-Bollinger, J. C. Cuevas, and N. Agraït, Quantum thermopower of metallic atomic-size contacts at room temperature, *Nano Lett.* **15**, 1006 (2015).
- [23] A. Ofarim, B. Kopp, T. Möller, L. Martin, J. Boneberg, P. Leiderer, and E. Scheer, Thermo-voltage measurements of atomic contacts at low temperature, *Beilstein J. Nanotechnol.* **7**, 767 (2016).
- [24] W. Lee, K. Kim, W. Jeong, L. A. Zotti, F. Pauly, J. C. Cuevas, and P. Reddy, Heat dissipation in atomic-scale junctions, *Nature (London)* **498**, 209 (2013).
- [25] L. A. Zotti, M. Bürkle, F. Pauly, W. Lee, K. Kim, W. Jeong, Y. Asai, P. Reddy, and J. C. Cuevas, Heat dissipation and its relation to thermopower in single-molecule junctions, *New J. Phys.* **16**, 015004 (2014).
- [26] L. Cui, R. Miao, K. Wang, D. Thompson, L. A. Zotti, J. C. Cuevas, E. Meyhofer, and P. Reddy, Peltier cooling in molecular junctions, *Nat. Nanotechnol.* **13**, 122 (2018).
- [27] J. C. Klöckner, M. Matt, P. Nielaba, F. Pauly, and J. C. Cuevas, Thermal conductance of metallic atomic-size contacts: Phonon transport and Wiedemann-Franz law, *Phys. Rev. B* **96**, 205405 (2017).
- [28] M. Bürkle and Y. Asai, How to probe the limits of the Wiedemann-Franz law at nanoscale, *Nano Lett.* **18**, 7358 (2018).
- [29] D. O. Möhrle, F. Müller, M. Matt, P. Nielaba, and F. Pauly, Statistical analysis of electronic and phononic transport simulations of metallic atomic contacts, *Phys. Rev. B* **100**, 125433 (2019).
- [30] A. Jain and A. J. H. McGaughey, Thermal transport by phonons and electrons in aluminum, silver, and gold from first principles, *Phys. Rev. B* **93**, 081206(R) (2016).
- [31] N. Mingo and L. Yang, Phonon transport in nanowires coated with an amorphous material: An atomistic Green's function approach, *Phys. Rev. B* **68**, 245406 (2003).
- [32] J. C. Klöckner, J. C. Cuevas, and F. Pauly, Transmission eigenchannels for coherent phonon transport, *Phys. Rev. B* **97**, 155432 (2018).
- [33] N. W. Ashcroft and N. D. Mermin, *Solid State Physics* (Harcourt, Inc., Orlando, 1976).
- [34] C. Campañá and M. H. Müser, Practical Green's function approach to the simulation of elastic semi-infinite solids, *Phys. Rev. B* **74**, 075420 (2006).
- [35] L. T. Kong, G. Bartels, C. Campañá, C. Denniston, and M. H. Müser, Implementation of Green's function molecular dynamics: An extension to LAMMPS, *Comput. Phys. Commun.* **180**, 1004 (2009).
- [36] L. T. Kong, Phonon dispersion measured directly from molecular dynamics simulations, *Comput. Phys. Commun.* **182**, 2201 (2011).
- [37] L. D. Landau and E. M. Lifshitz, *Statistical Physics Part 1*, 3rd ed. (Butterworth-Heinemann, Oxford, 1980).

- [38] F. Guinea, C. Tejedor, F. Flores, and E. Louis, Effective two-dimensional Hamiltonian at surfaces, *Phys. Rev. B* **28**, 4397 (1983).
- [39] F. Pauly, J. K. Viljas, U. Huniar, M. Häfner, S. Wohlthat, M. Bürkle, J. C. Cuevas, and G. Schön, Cluster-based density-functional approach to quantum transport through molecular and atomic contacts, *New J. Phys.* **10**, 125019 (2008).
- [40] M. Bürkle, T. J. Hellmuth, F. Pauly, and Y. Asai, First-principles calculation of the thermoelectric figure of merit for [2,2] paracyclophane-based single-molecule junctions, *Phys. Rev. B* **91**, 165419 (2015).
- [41] S. Plimpton, Fast parallel algorithms for short-range molecular dynamics, *J. Comput. Phys.* **117**, 1 (1995).
- [42] LAMMPS Molecular Dynamics Simulator, <http://lammps.sandia.gov>.
- [43] M. W. Finnis and J. E. Sinclair, A simple empirical  $N$ -body potential for transition metals, *Philos. Mag. A* **50**, 45 (1984).
- [44] G. J. Ackland, G. Tichy, V. Vitek, and M. W. Finnis, Simple  $N$ -body potentials for the noble metals and nickel, *Philos. Mag. A* **56**, 735 (1987).
- [45] J. W. Lynn, H. G. Smith, and R. M. Nicklow, Lattice dynamics of gold, *Phys. Rev. B* **8**, 3493 (1973).
- [46] N. Mingo, Anharmonic phonon flow through molecular-sized junctions, *Phys. Rev. B* **74**, 125402 (2006).
- [47] R. H. M. Smit, C. Untiedt, A. I. Yanson, and J. M. van Ruitenbeek, Common Origin for Surface Reconstruction and the Formation of Chains of Metal Atoms, *Phys. Rev. Lett.* **87**, 266102 (2001).
- [48] A. I. Yanson, G. Rubio-Bollinger, H. E. van den Brom, N. Agraït, and J. M. van Ruitenbeek, Formation and manipulation of a metallic wire of single gold atoms, *Nature (London)* **395**, 783 (1998).
- [49] N. Agraït, C. Untiedt, G. Rubio-Bollinger, and S. Vieira, Onset of Energy Dissipation in Ballistic Atomic Wires, *Phys. Rev. Lett.* **88**, 216803 (2002).